HETGS Calibration Update

Herman Marshall

A new set of HETGS efficiencies was released as part of CalDB v4.4.7, which should reduce systematic differences between the HEG and MEG fluxes as well as improve overall model fits. Here, I'll summarize the steps that went into the release and what is in store for the next update. Details will be available at the HETGS calibration web site *http://space.mit.edu/ASC/calib/hetgcal.html* and will be presented at the next meeting of the International Astronomical Consortium for High Energy Calibration (IACHEC) in March (see *http://web.mit.edu/iachec/meetings/index.html*). First, data were selected from the TGCat online catalog of HETGS spectra. See *http://tgcat.mit.edu* to obtain the data used here. I started with sources of all sorts but relied most on those with simple continua. Next, the +1 and −1 fluxes were compared for both MEG and HEG in order to verify that 1) the chip QEs are consistent and 2) that contamination correction of one grating "arm" is consistent with the other (because there is a spatial variation to the contaminant's thickness). All fluxes came out to be consistent to within 1% on average except near 0.5 keV, where the two sides differ by 3–5% but generally within the statistical uncertainties.

Fig. 1 shows the ratio of the MEG and HEG fluxes as a function of wavelength, binned to have 1% uncertainties so that small systematic errors may be found and corrected. Because the polynomial fit can correct only the ratio of the MEG and HEG efficiencies, I allocated the correction to either the HEG or MEG efficiencies: longer than a specified wavelength, all corrections are applied to the HEG, while for shorter wavelengths, the MEG is corrected. The simple reasoning behind the choice is that it was somewhat easier to determine HEG efficiencies on the ground at high energies due to the higher resolution while harder to measure them at low energies due to significantly lower effective area. Furthermore, the HEG part of the HETGS dominates observations at high energy while the MEG part dominates at low energy, so a "least harm" dictum suggests applying less correction where a grating part dominates. I tried several possible cross-over wavelengths

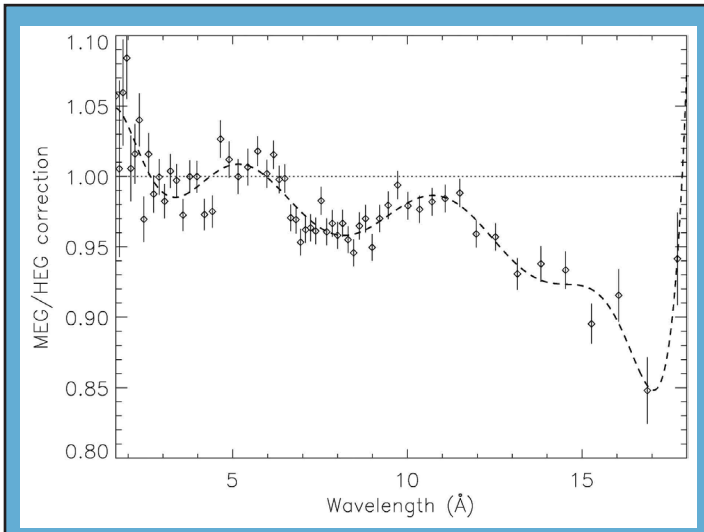

Fig. 1 - The ratio of the MEG and HEG fluxes as a function of wavelength, binned to have 1% uncertainties or bin widths less than 5% of the central wavelength. The sense of the correction is that the values shown should be applied to the MEG efficiencies to bring MEG fluxes into agreement with those derived from HEG data. The dashed line is a 9th order polynomial fit to the data.

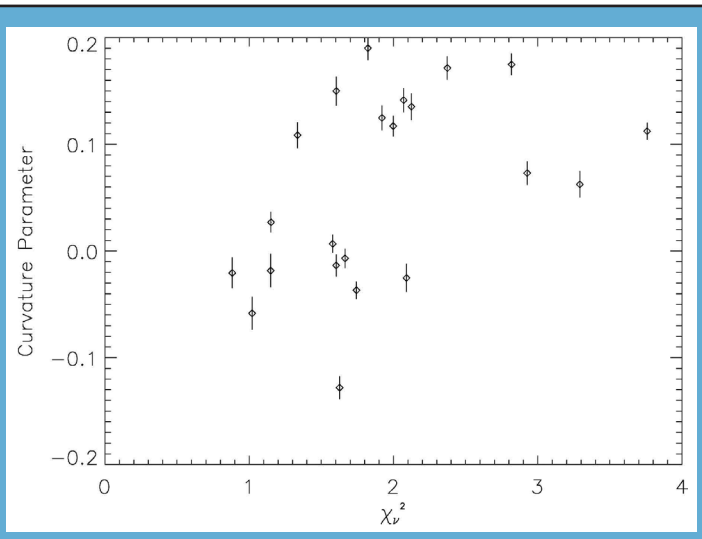

Fig. 2 (above)- The curvature parameter β, as a function of reduced χ^2 for fits to HETGS spectra of AGN. See Eq. 1 for the model, which defines β.

Fig. 3 (below)- The average residuals for curved power law fits to the HETGS data for 8 BL Lac objects. For most of the HETGS range, the systematic deviations are not significant or are less than 3%. Deviations of 5–10% near 6 keV and 0.7 keV will be investigated further.

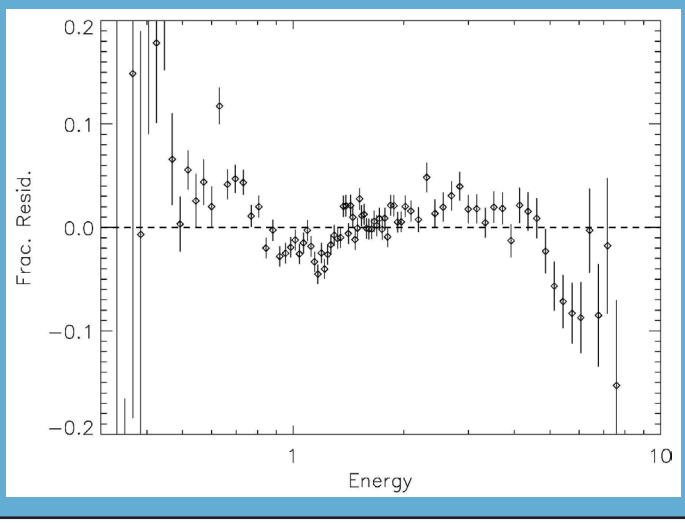

and found that 10 Å minimized the reduced χ^2 in BL Lac fits (see below).

For about 20 observations of AGN, I applied the new corrections to the HETGS spectra and fit them to a simple logarithmic parabola model with four parameters:

Eq. 1 $$n_E = A e^{-N_H \sigma(E)} E^{-\Gamma+\beta \log E}$$

where N_H was fixed for each AGN to an estimate based on 21 cm data (the results are robust against the exact choice), and the overall model is a power law with a curvature term, β. The model is the same as that used for BL Lac objects by Perlman et al.[1]. The curvature term is negative for spectra that are convex upward and positive for those with soft or hard excesses. Fig. 2 shows that the quality of the fit is related to the value of β: better fits are obtained for negative curvature. The fits with positive curvature were predominantly radio-loud AGN with emission lines, indicating that these spectra are actually more complex than a simply curving model provides. For the remaining analysis, the sources with $\beta < 0.3$ were chosen; these were the BL Lac objects PKS 2155-304 and 1H 1426-428. The curvature values are similar to those found for other BL Lac objects[1].

The spectral residuals for the BL Lac objects were combined in order to see if there were significant remaining residuals. Fig 3 shows the result. While there are possible systematic errors of up to 5% over the 0.5–7 keV range, most of the deviations are less than 3%. Residuals to simple fits to the other AGN (not shown) are also less than 3% over most of the 0.5–7 range and only as large as 5% near 0.7 keV. Thus, an approximate limit to relative systematic errors is about 3–5% over the HETGS range. While these residual errors will be examined further to see if they can be eliminated, another area of investigation will be the cross-dispersion selection efficiency, which is currently applied in the grating RMFs.

Recent HETGS Highlights

The High Energy Transmission Grating Spectrometer continues to provide excellent spectra for detailed examination of source properties. Over the past year, papers have appeared on warm ionized winds in AGN [2, 3, 8], the distance and dust to Cyg X-1[7], O star winds [5,6], and an accretion shock at the surface of V2129 Oph, a classical T Tauri star [4].

The T Tauri result is highlighted in Fig. 4, which shows the spatial distribution of the two X-ray emitting plasma components of V2129 Oph. Left and right cartoons correspond to the viewing angles of two *Chandra* observing segments, with observer in the rightward direction [4]. Red region marks the post-shock high density plasma at 3–4 MK, blue regions indicate low density coronal plasma with T ranging from 2 up to ~30 MK. The emission measure (EM) distributions derived from HETGS spectra corresponding to the two observing segments. Red EM bins symbolize observed EM values ascribed to post-shock plasma, while blue bins represent those accounting for coronal plasma. During segment 1, the pre-shock material does not block the view of both post-shock and coronal plasma: the EM distribution is therefore the sum of the EM distributions of the two components. During segment 2, the pre-shock material almost completely absorbs the X-rays of the post-shock plasma emitted toward the observer, while coronal emission is mostly unaffected: in this case, all the X-rays detected are those produced by coronal plasma; the reconstructed EMD, being only those of coronal plasma, hence misses the high EM values at 3–4 MK.

References

[1] Perlman, E. S., et al. (2005). ApJ 625:727.
[2] Zhang, S. N., Ji, L., Marshall, H. L., et al. (2011). MNRAS 410:2274.
[3] Mocz, P., Lee, J. C., Iwasawa, K., & Canizares, C. R. (2011). ApJ 729:30.
[4] Argiroffi, C., Flaccomio, E., Bouvier, J., et al. (2011). A&A 530:A1.
[5] Mitschang, A. W., Schulz, N. S., Huenemoerder, D. P., Nichols, J. S., & Testa, P. (2011). ApJ 734:14.
[6] Cohen, D. H., Gagné, M., Leutenegger, M. A., et al. (2011). MNRAS 415:3354.
[7] Xiang, J., Lee, J. C., Nowak, M. A., & Wilms, J. (2011). ApJ 738:78.
[8] Zhang, S.-N., Gu, Q.-S., Ji, L., & Peng, Z.-X. (2011). Research in Astronomy and Astrophysics 11:1171.

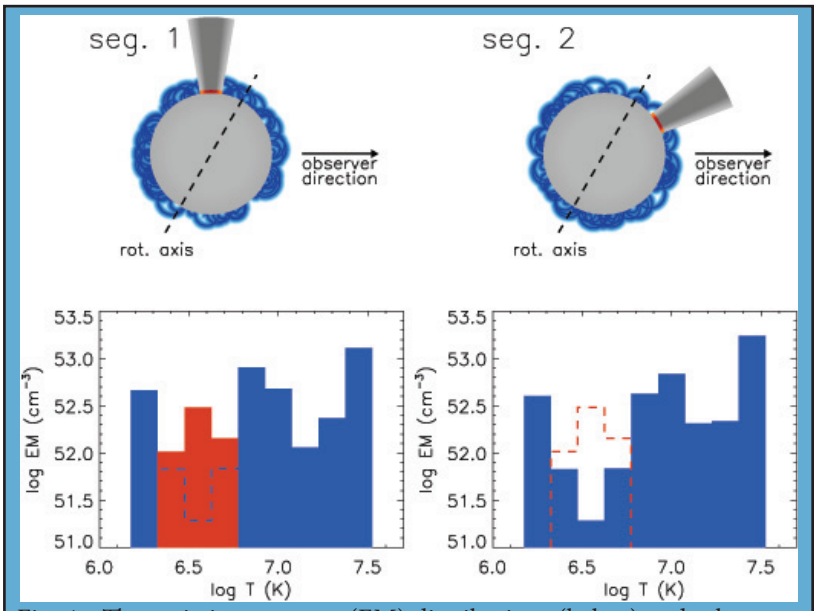

Fig. 4 - The emission measure (EM) distributions (below) and schematics of the physical model (above) are shown for two observations of the classical T Tauri star V2129 Oph. Most of the emission is from coronal gas (blue). EM with T of 3–4 MK is attributed to the base of the accretion stream (right panel, in red), observable in segment 1 but obscured by the upper part of the accretion stream during the 2nd observation (dashed red line in lower right panel). See Argiroffi et al. [4] for details.